Experimental Investigation on Corrosion Abatement in Straw Combustion by Fuel Mixing

ARTICLE *in* ENERGY & FUELS · MAY 2011

Impact Factor: 2.79 · DOI: 10.1021/ef200232r

CITATIONS
15

READS
38

8 AUTHORS, INCLUDING:

Roger Antoine Khalil
SINTEF
20 PUBLICATIONS **215** CITATIONS
SEE PROFILE

Ehsan Houshfar
Norwegian University of Science and Techno…
21 PUBLICATIONS **107** CITATIONS
SEE PROFILE

Øyvind Skreiberg
SINTEF Energy Research, Trondheim, Norway
76 PUBLICATIONS **831** CITATIONS
SEE PROFILE

Terese Løvås
Norwegian University of Science and Techno…
31 PUBLICATIONS **134** CITATIONS
SEE PROFILE

energy&fuels

ARTICLE

pubs.acs.org/EF

Experimental Investigation on Corrosion Abatement in Straw Combustion by Fuel Mixing

Roger A. Khalil,*[,†] Ehsan Houshfar,[‡] Wilson Musinguzi,[‡] Michaël Becidan,[†] Øyvind Skreiberg,[†] Franziska Goile,[†] Terese Løvås,[‡] and Lars Sørum[†]

[†]Department of Energy Processes, SINTEF Energy Research, NO-7465 Trondheim, Norway

[‡]Department of Energy and Process Engineering, Norwegian University of Science and Technology (NTNU), NO-7491 Trondheim, Norway

ABSTRACT: In an attempt to minimize corrosion in biomass-fired boilers, combustion experiments were performed using binary mixtures of straw with peat, sewage sludge, or grot (branches and treetops). The mixing ratios were carefully selected using literature and thermodynamic calculations. All mixtures were pelletized. The combustion experiments were performed in a laboratory-scale multi-fuel reactor. Extensive analytical analysis of the system included the gas concentration and particle size distribution in the flue gas, the elemental composition of the fuel, and the bottom ash and specific particle size fractions of fly ash. This allowed for the determination of the fate of the main corrosive compounds, in particular, chlorine. The corrosion risk associated with the three fuel mixtures was quite different. Grot was found to be a poor corrosion-reduction additive because of its marginal influence on the chlorine share in aerosols. Grot could not serve as an alternative fuel for co-firing with straw either because no dilution effect on the particle load was measured. Peat was found to reduce the corrosive compounds only at high peat additions (50 wt %). Sewage sludge was the best alternative for corrosion reduction because 10 wt % addition almost eliminated chlorine from the fly ash.

INTRODUCTION

According to the world energy outlook of the International Energy Agency (IEA), the total energy consumption in the world will increase by a rate of 1.5% per year until 2030.[1] Fossil fuels produce the major greenhouse gas, CO_2, when they are used for electricity or heat production. Biomass, which is already the main contributor to renewable energy, is expected to further increase its share in three key sectors: heat and power, transportation fuels, and production of bioproducts. Energy conversion from biomass is close to being CO_2-neutral; however, biomass use will most likely result in the emission of other types of pollutants. An increased number of biomass energy plants are looking into cutting down their costs using cheaper feedstock alternatives, i.e., herbaceous and agricultural biomass, energy crops, waste wood, municipal solid waste, etc. These types are usually continuously produced locally and are likely to be available within a reasonable vicinity of the power plant, which is quite advantageous in terms of fuel transport cost reduction. However, these types of feedstock usually have a higher ash content compared to wood, and in addition, they are composed of higher concentrations of problematic ash compounds. For example, straw (the main focus of this work) contains high quantities of chlorine and alkali metals. This combination creates severe corrosion problems in combustion systems. Straw is also known to cause slagging and fouling because of a relatively low ash melting temperature.[2] In fluidized-bed systems, low-temperature ash melting can also cause agglomeration of bed material, resulting in defluidization of the bed.[3]

Dependent upon the chemical composition of the ash, the products of combustion for chlorine are mainly hydrogen chloride (HCl), Cl_2, alkali chlorides (KCl and NaCl), and zinc and lead chlorides ($ZnCl_2$ and $PbCl_2$).[4] In the boiler section of the biomass combustion plants, especially at the surface of superheater tubes, the subsequent cooling of the flue gas results in the condensation of alkali chlorides.[5] In the same manner, zinc and lead chlorides may have a major corrosive effect in boilers because of their relatively lower melting temperature, in addition to their ability to form low-temperature eutectics that, in return, facilitate corrosive reactions furthermore.[6] HCl, on the other hand, plays part in the formation of polychlorinated dibenzo-*p*-dioxins (PCCDs) and polychlorinated dibenzofurans (PCDFs), which are halogenated organic compounds that are considered to be extremely toxic.[7] However, from a corrosion point of view, HCl is the favorable compound to produce because it is expected to escape the heat-exchange section without condensing. HCl can, in addition, be easily removed from the flue gas through sorption (dry or in activated carbon) or with scrubbers (using limestone).[8]

The importance of avoiding alkali chlorides in the boiler becomes clear when understanding the corrosion mechanism. High-temperature Cl-induced corrosion may be described as such: as metal chlorides condense on the iron surface, Cl_2 can be formed by chemical reactions with gaseous compounds. Cl_2 diffuses to the superheater tubes of the boiler and reacts with iron to form ferrous chloride ($FeCl_2$). Because of the high steam pressure, $FeCl_2$ migrates and evaporates toward the flue gas, where it reacts with oxygen and forms iron oxide. In this process, Cl_2 is regenerated and again ready to react with the iron surface.[4,7] The chlorine is therefore recycled to the metal surface, where it participates continuously with the iron stripping of the

Received: February 14, 2011
Revised: May 12, 2011
Published: May 12, 2011

Table 1. Proximate Analysis of the Different Fuels and Fuel Mixtures (wt %, db)[a]

	ash	volatile matter	fixed carbon	moisture	HHV (MJ/kg)
straw(80)G(20)	4.4	77.9	17.7	13.8	20.2
straw(50)G(50)	3.7	77.5	18.9	11.8	20.7
grot(100)	2.3	77.0	20.7	9.6	21.8
straw(90)S(10)	7.9	76.6	15.5	9.3	20.0
straw(80)S(20)	11.9	73.6	14.6	9.4	20.0
straw(80)P(20)	5.9	77.1	17.1	14.4	20.4
straw(50)P(50)	7.4	73.1	19.5	17.1	21.3

[a] In the first column, G, grot; S, sewage sludge; and P, peat.

superheater tubes. To reduce chlorine corrosion, several methods exist, although none of them can claim to completely remedy this problem. Corrosion reduction can be attained through (i) fuel leaching (washing of biomass to decrease the Cl content),[9] (ii) automated and continuous cleaning of boiler parts, (iii) coatings and corrosion-resistant materials, (iv) lower steam parameters, although this will result in reduced efficiency, or (v) modification of the elemental composition of the fuel by mixing different biomasses or using additives to alter the ash chemistry. The latter is actively researched because of the complexity of the chemistry involved. Among these studies, it is worth mentioning the work on biomass fuel mixing,[10−12] the co-firing of risky biomass with non-problematic fuels,[13−17] and the use of additives.[18−23] The aim is to capture the alkali metals through several possible paths and thereby prevent the formation of alkali chlorides. Different ash elements are capable of capturing alkalis, among these are aluminum silicates, phosphates, and sulfur. For sulfur, the reaction with alkali chlorides is possible with either SO_2 or SO_3 according to eqs 1 and 2 and where M could be either K or Na.

$$2MCl + SO_2 + H_2O + 1/2O_2 \rightarrow M_2SO_4 + 2HCl \quad (1)$$

$$2MCl + SO_3 + H_2O \rightarrow M_2SO_4 + 2HCl \quad (2)$$

Reaction 1 is very slow compared to the sulfation reaction (eq 2). This makes the formation of SO_3 the limiting step for the capture of alkalis.[5,24] SO_3 formation can happen in boilers through different sulfur sources, among these are SO_2, aluminum sulfate $[Al_2(SO_4)_3]$, iron sulfate $[Fe_2(SO_4)_3]$, and ammonium sulfate $[(NH_4)_2SO_4]$.[25] The so-called ChlorOut system developed and patented by Vattenfall uses a spraying solution of ammonium sulfate prior to the superheater section in the boiler as a means of alkali capture.[26] Phosphorus may also contribute to alkalis capture directly or by making sulfur more available through the formation of calcium phosphates because calcium would otherwise form calcium sulfate.[27,28] The dominating crystalline phases containing potassium and phosphorus have been identified as $CaK_2P_2O_7$ and $MgKPO_4$ in ash from combustion of cereal grains.[14,27] The aluminum silicate sources are many and will not be mentioned in details in this paper. Kaolin ($Al_2O_3 \cdot 2SiO_2 \cdot 2H_2O$) is an example of an additive based on aluminum silicate that can capture alkalis in both reducing and oxidizing atmospheres. Many different alkali aluminum silicates may be formed; i.e., leucite ($KAlSiO_6$) and kalsilite ($KAlSiO_4$) have been observed.[29]

Table 2. Elemental Composition of the Different Fuels and Fuel Mixtures (wt %, daf) in Addition to Cl and S (wt %, db)[a]

	C	H	O	N	S	Cl
straw(80)G(20)	50.2	6.1	42.8	0.48	0.20	0.17
straw(50)G(50)	51.4	6.1	41.7	0.46	0.17	0.12
grot(100)	53.4	6.2	39.9	0.43	0.12	0.04
straw(90)S(10)	49.4	6.2	42.9	0.93	0.34	0.19
straw(80)S(20)	49.3	6.3	42.3	1.40	0.47	0.19
straw(80)P(20)	50.7	6.1	41.9	0.89	0.24	0.17
straw(50)P(50)	52.6	6.1	39.4	1.51	0.27	0.11

[a] In the first column, G, grot; S, sewage sludge; and P, peat.

The complexity of the ash chemistry during combustion has led to the creation of several indices to quantify the corrosion risk. These indices take into account elements capable of capturing alkalis and relate it to the problematic elements or compounds in the fuel. For example, a S/Cl molar ratio of 4−6 is expected to decrease the mass flow of Cl in the fine fly ash, whereas S/Cl values lower than 2 are considered to give a high corrosion risk.[15,24] The excess of sulfur compared to alkalis is considered in the molar ratio $2S/(K + Na)$, while other forms of the same ratio incorporating Ca exist $[2S/(2Ca + K + Na)]$. Ca incorporation is of importance because it can form $CaSO_4$, thereby prohibiting sulfur from capturing alkali. Similar ratios exist emphasizing the aluminum silicate ability to capture alkalis.[14,30] As an example, the minimum suggested value for the $(Al + Si)/Cl$ molar ratio is 8−10 to avoid chlorine deposition on heat-exchange surfaces.[31] Although such indices are a practical tool for a general evaluation of the relative risk of chlorine-induced corrosion, the authors feeling is that these ratios should be used carefully and that they may not reflect precisely the real life corrosion risk.

In this work, the abatement of corrosion in straw combustion is studied. Peat and sewage sludge were chosen as fuel additions to straw because of their rich nature in sulfur and aluminum silicates. Grot was chosen as a fuel additive for two reasons: (i) to serve as a reference experiment to compare to the other additives because pure straw could not be used as a result of problems with slagging at the selected temperature and (ii) to check if it could serve as a dilution fuel to lower the concentration of unwanted compounds. The different fuels and the rate of mixing were carefully chosen based on the literature and thermodynamic calculations, with the sole purpose of minimizing the corrosion risk.

MATERIALS AND METHODS

Sample Preparation. The biomass fuels used in this experimental campaign were obtained from different sources. The straw and sewage sludge were acquired through the SciToBiCom ERA-net bioenergy scheme activity. Peat was provided by Eidsiva Bioenergi AS. In addition, a mixture of branches and tops (grot) was provided by The Norwegian Forest and Landscape Institute. The Norwegian word grot is hereafter used for the biomass fuel referred to as "branches and treetops". The fuels were grinded in a mill to produce a maximum particle size of 2−3 mm. The different fuels were mixed and pelletized in a laboratory-scale pellet machine. The produced pellets had a diameter of 6 mm and a length of 5−15 mm and were air-dried before they were used in experiments. Only binary mixtures were studied in this work. The compositions of the mixtures are shown in Table 1. For all tables and figures, the first bracketed number in the code word of each experiment

Table 3. Main Elements in Ash (wt %, db)[a]

Si	Al	Ca	Fe	K	Mg	Mn	Na	P	Ti	Zn	Pb
1.06	0.01	0.39	0.01	0.70	0.07	0.01	0.02	0.08		18.6	0.49
0.73	0.01	0.47	0.01	0.55	0.07	0.03	0.02	0.06		41.3	0.73
0.24	0.02	0.65	0.02	0.28	0.05	0.07	0.03	0.05		77.3	0.94
1.59	0.15	0.64	0.59	0.76	0.12	0.01	0.03	0.44	0.01	85.7	2.45
1.82	0.32	0.96	1.24	0.71	0.17	0.01	0.05	0.85	0.03	171	4.52
1.50	0.10	0.52	0.10	0.75	0.09	0.01	0.02	0.10		6.7	0.59
1.94	0.38	0.69	0.29	0.52	0.09	0.01	0.07	0.08	0.01	9.14	1.80

[a] The fuel sequence is the same as in the previous tables. Zn and Pb are in mg/kg (db).

Table 4. Corrosion Indicators for the Different Fuel Mixtures[a]

	S/Cl	2S/(K + Na)	(Al + Si)/(K + Na)	(Al + Si)/Cl
straw(80)G(20)	1.4	0.6	2.2	9.5
straw(50)G(50)	1.7	0.7	1.9	9.4
grot(100)	3.8	0.9	1.1	9.1
straw(90)S(10)	2.4	1.1	3.1	13.8
straw(80)S(20)	3.7	1.6	4.0	18.6
straw(80)P(20)	1.7	0.8	3.0	12.8
straw(50)P(50)	2.8	1.2	4.7	21.7

[a] In the first column, G, grot; S, sewage sludge; and P, peat.

represents the weight percent of straw, while the second number gives the percentage of the added fuel. S stands for sewage sludge; P stands for peat; and G stands for grot. The proximate analyses of the samples (Table 1) were carried out according to the standard methods ASTM E871, ASTM E872, and ASTM D1102. The fixed carbon was calculated by difference to 100%. The ultimate analysis and the higher heating value (HHV) (calculated on the basis of the elemental composition of the fuel) are presented in Table 2. A chemical analysis of the ash content of the primary fuel and all of the blends was determined by inductively coupled plasma−atomic emission spectrometry (ICP−AES) and inductively coupled plasma−sector field mass spectrometry (ICP−SFMS). Table 3 shows the composition of the main ash constituents for the different fuel mixtures, while Table 4 shows some corrosion indicator molar ratios for the respective fuels. In all mixtures, the S/Cl molar ratio is below 4 (Table 4), which is the lowest recommended ratio to avoid severe corrosion. The ratio 2S/(K + Na) for the different mixtures is between 0.6 and 1.6, which is also well below the recommended value of 4. The aluminum silicate ratios for the fuel mixtures also lie below recommended values. However, the indicators do not take into consideration the full complexity of the ash chemistry during combustion and should not be regarded as very reliable concerning corrosion abatement. A better predictive tool for the relative corrosion risk of the fuel mixtures used in this study is thermodynamic equilibrium calculations (not presented here). Such calculations for straw mixed with grot, sludge, or peat were performed for a mixing range of 5−95%. The mixing levels selected for the experimental campaign are based on these calculations as well as the literature, with the purpose of minimizing the formation of corrosive compounds in straw-fired boilers. The results of equilibrium calculations are discussed in detail in another paper.[32]

Experimental Setup. The experiments were carried out in an electrically heated laboratory-scale multi-fuel reactor. Its schematic drawing is presented in Figure 1. The setup used is able to generate close to identical conditions for the combustion of the different fuel mixtures, providing a good platform where the formation of corrosive

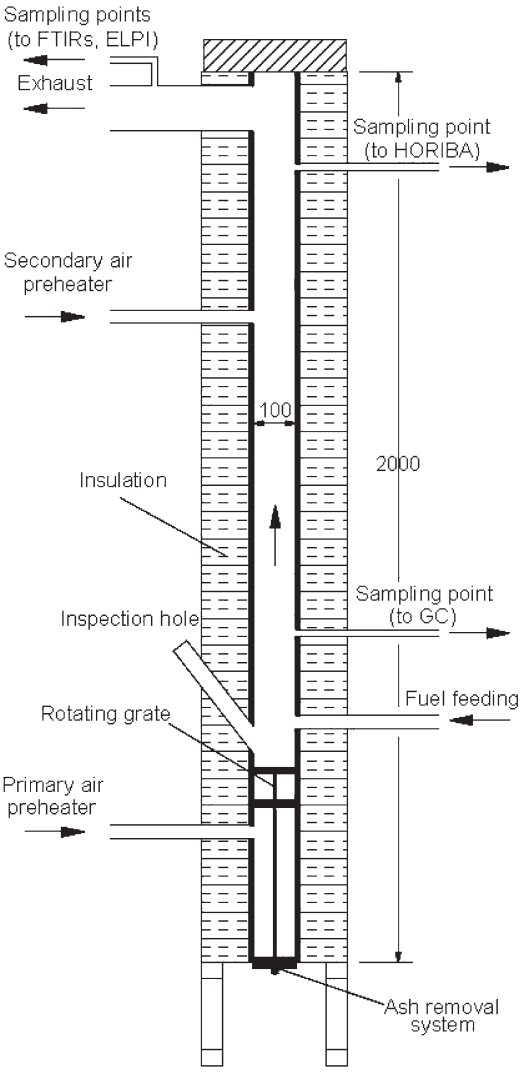

Figure 1. Schematic drawing of the laboratory reactor.

compounds from the different fuel mixtures could be easily compared. The reactor has a ceramic inner tube (100 mm diameter). The altogether 2 m high vertical tube consists of two 1 m ceramic tubes connected with a ceramic socket. The ceramic tubes are made of nonporous and noncatalytic alumina. The reaction section, located above the grate, is 1.6 m long, while the section below the grate is 0.4 m long. The reactor heating system is fitted inside the insulation shell and consists of four separate 0.5 m high heating zones of 4 kW each (16 kW in total) that enclose the ceramic tube. The combustion air is preheated to the reactor temperature by external preheaters. The primary air is added under the grate, and the secondary air is added above the grate. The distance between the grate and the secondary air supply is 865 mm, corresponding to a residence time of 19 s. The air flow is controlled by two high-precision digital mass flow controllers. The lower part of the multi-fuel reactor contains a two-grate system (10 cm apart): a primary grate and a final burnout grate, as well as an ash collection system. Both grates and the ash bin are made of Inconel. The two-level design of the grate also permits fuel staging. Both the reactor flue gas composition and the composition of the fuel gas after the primary zone, as well as the particle emission size distribution, were continuously monitored. A schematic diagram of the sampling lines is shown in Figure 2. For gas analysis in the primary zone, a micro gas chromatograph (GC) was used. The exhaust gases were quantified

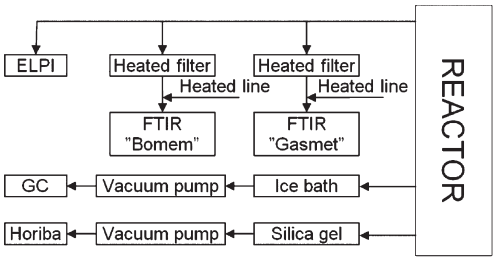

Figure 2. Schematic diagram of the sampling system.

online with two different Fourier transform infrared (FTIR) instruments and where the extracted gases were passing through heated filters and heated lines. To detect instabilities during combustion, an online gas analyzer with a fast response time was also deployed. A partial flow was taken through a sampling point near the top of the reactor. The analyzer is a portable stack gas analyzer that can simultaneously measure CO, SO_2, CO_2, O_2, and NO_x. The particle size distribution and concentration in the flue gas were measured by an electrical low-pressure impactor (ELPI). A partial stream of flue gas was collected through a stainless-steel probe located in the flue gas stack. The flue gas was then led through a double diluter system to the ELPI. The instrument is a real-time particle size analyzer for monitoring aerosol particle size distribution. The ELPI measures the airborne particle size distribution in the range of 0.03−10 μm with 12 stages and a time resolution of 1 s. The nominal air flow is 10 L/min, and the lowest stage pressure is 100 mbar. The ELPI operates at ambient temperature, while the gas sample is taken at a temperature of 110 °C. The dilution ratio is approximately 80, while the particle concentration in the diluted stream is about 3.9×10^5 particle/cm^3. The aerosol samples were collected on aluminum plates. The plates were covered by a thin layer of vaseline to provide a sticky surface. The chemical analyses of the samples were made by energy-dispersive X-ray analysis connected to a scanning electron microscope (SEM/EDX). The total mass of the particles on each plate was 10−100 μg. For each run, four plates with the particle sizes (D50%) of 0.093, 0.26, 0.611, and 1.59 μm were chosen for SEM/EDX analysis. Five EDX spot analyzes were selected from different locations on each plate. The elements detected by the analysis were C, O, Na, Mg, Al, Si, P, S, K, Ca, Cl, Fe, Zn, and Pb. After standard ZAF correction, the analysis was normalized to 100% by weight. The signals for carbon, oxygen, and aluminum cannot be used for quantitative information because their signals are disturbed by various experimental sources. The variation among the five analyses for each plate was negligible, indicating that the particles in the piles were homogeneous. The main components in the analyzed particles were K, S, Cl, and Na (Figure 6). On average, 80 wt % of the oxygen-free samples (excluding C and Al) consisted of these four elements. Zn and Pb constituted on average of 14 wt %, whereas the portion of the inert oxide-forming elements (Si, Ca, Fe, P, Mg, and Cr) was 6 wt %. P and Mg concentrations were very low in all samples. The portion of inert metals was considerably higher in the larger particles compared to the smaller fractions, indicating that the compounds of these metals (oxides) originate from the original fuel ash and have not originated from devolatilization. Lead and zinc are partly in oxide form and partly in salt form. The oxides are almost certainly ZnO and PbO. The salt part was made of sulfate and chloride of K, Na, Zn, and Pb. The crucial step of the data treatment was to estimate the compounds in which the elements were studied. This consideration was based on a recently published study on aerosol formation in combustion.[23] The assumptions regarding the speciation can be explained as follows: (i) Potassium and sodium are as chlorides or sulfates, because alkali is volatilized as hydroxides or chlorides and some of the alkali is sulfated at high temperatures. (ii) Silicon, calcium, iron, magnesium, and chromium

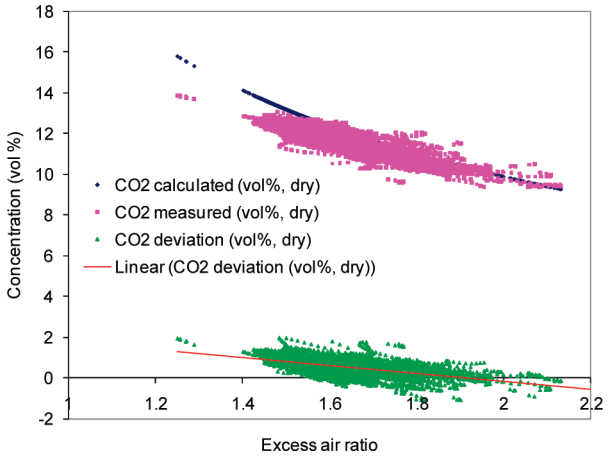

Figure 3. CO_2 concentration for the reference experiment with grot. A comparison between measured and calculated values.

are as oxides, because these are nonvolatile and these elements do not form sulfates or chlorides at higher temperatures (except Ca, which forms sulfate and phosphate, but in the present case, Ca content in the samples is low). (iii) Zinc and lead can both be as oxides and/or chlorides and sulfates. Two chemical fractions in the fly ash samples were then defined: an "inert" part constituted of high-melting insoluble oxides (SiO_2, CaO, Fe_2O_3, MgO, P_2O_5, Cr_2O_3, ZnO, and PbO) and a "salt" part consisting of low-melting water-soluble chlorides and sulfates (K, Na, Zn, Pb, Cl_2, and SO_4). The salt fraction is the one causing corrosion and deposition problems in the superheater area. It is evident that the salt part must have a balance between cations and anions. Thus, because the amount of Cl, S (as SO_4), K, and Na is known from chemical analysis of the fly ash samples, the portion of Zn and Pb can be determined by difference. The notation K_2, Na_2, and Cl_2 are used for consistency with $ZnCl_2$ and $PbCl_2$. "S" should be read as "SO_4".

Experimental Procedure. All experiments in this work were carried out employing staged air combustion and isothermal conditions. The reactor and the primary and secondary air inputs were preheated to 850 °C prior to the startup of the experiment. The pellets were fed semicontinuously from a rotating battery of fuel containers using a pneumatically driven piston. The feeding frequency was set to ensure a feeding rate of 400 g/h. The pellets are primarily combusted on the upper grate. The pellets are gradually moved to a slot leading to the second grate by rotating blades. Each grate has two rotating blades moving at a speed of 3 min/round. The final burnout takes place on the second grate before the ash is moved to a slot from where it falls into the ash bin. At the bottom of the ash bin another rotating blade moves the ash into an ash container. Because of minor variations in the pellet size, it was not possible to feed exactly the target rate of 400 g/h. Hence, the supply of primary air could not be regulated accurately to attain the set substoichiometric condition of 0.8, although the variations were within an acceptable range (0.7−0.9). The primary air supply was adjusted, so that the CO concentration from the primary zone was approximately 3%. The flow of the secondary air supply was adjusted to an overall excess air ratio of 1.6 in the stack.

RESULTS AND DISCUSSION

The amount of unburnt gas was very low (typically below 50 ppm CO at 11% O_2 in dry flue gas). However, during an initial stabilization period and short periods of high fluctuation in the fuel feeding, the excess air ratio deviated from the target value of 1.6. During such periods, the CO emission level increased to

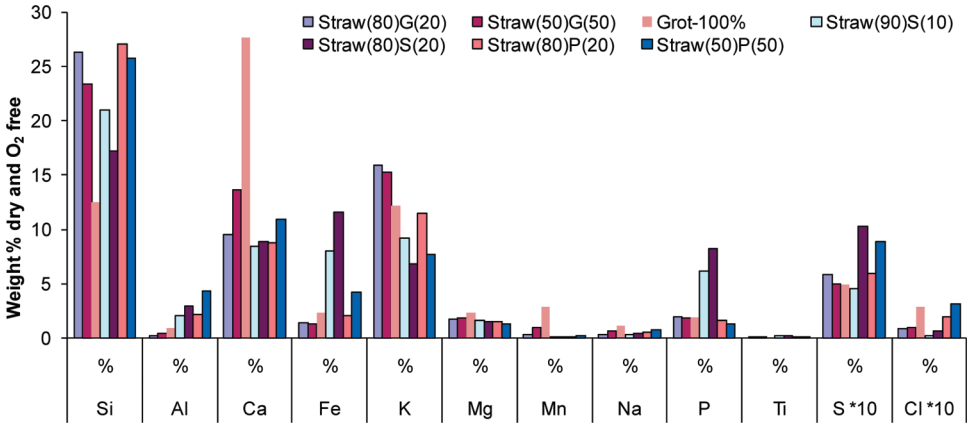

Figure 4. Major composition of bottom ash from all experiments (in the legend, G, grot; S, sewage sludge; and P, peat).

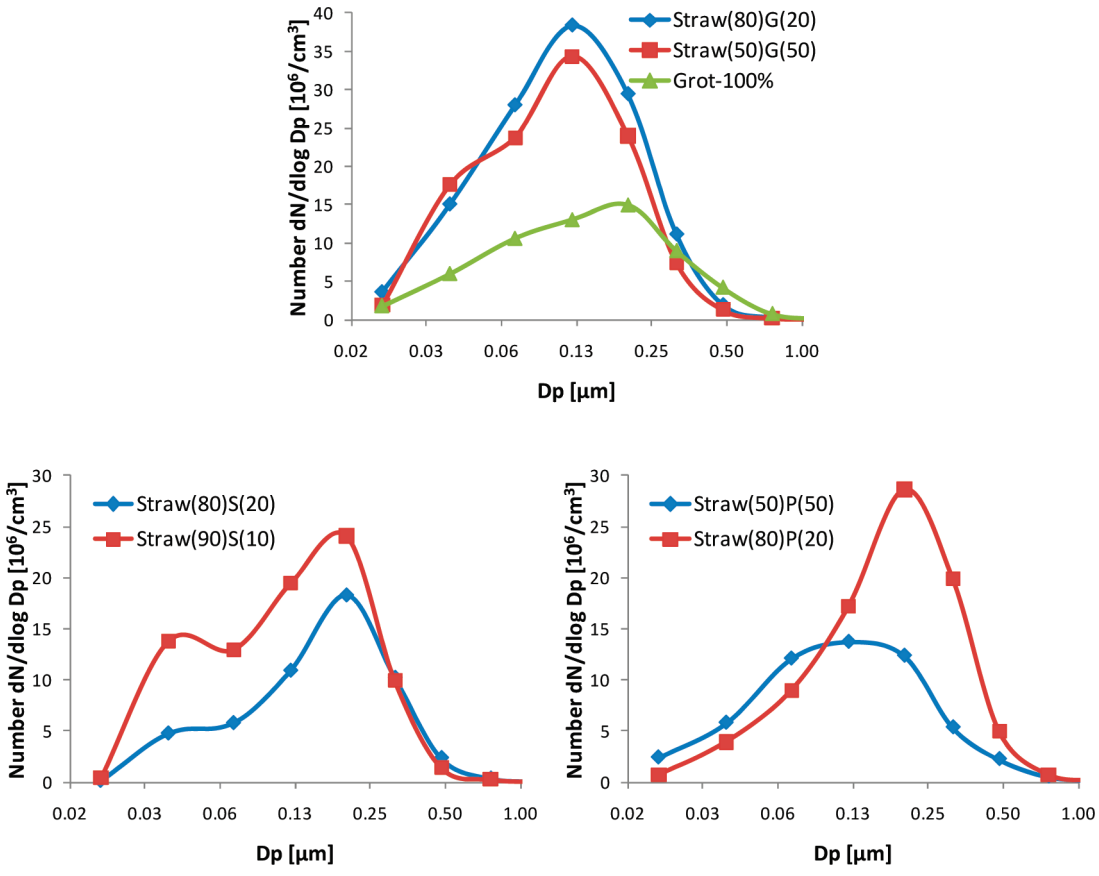

Figure 5. Particle size distribution in the fly ash (0−1 μm) for the three binary mixtures (in the legend, G, grot; S, sewage sludge; and P, peat).

typically 200 ppm at 11% O_2 in dry flue gas. The combined emission levels of hydrocarbons were typically below 5 ppm at 11% O_2 in dry flue gas. The accurate control of the fuel feed and the combustion air made it possible to check the carbon and hydrogen balance by calculating the CO_2 and H_2O concentration from the known fuel composition. The overall balance was corrected for the unburned carbon in the bottom ash (collected after the experiments) by weighting the ash before and after exposing it to a temperature of 550 °C for 20 h. The calculated carbon and hydrogen balances were used to remove outliers in the measured concentrations. Figure 3 shows the carbon balance as a function of the excess air ratio for the experiment with grot. The deviation between the calculated and measured value was within a 2% range; this was the case for all of the experiments performed in this study.

Bottom Ash Analysis. To assess the fate of key ash elements during biomass combustion and the possible effects of fuel mixing, the chemical composition of the bottom ash was determined by ICP−AES and ICP−SFMS. The concentrations of the most important elements are shown in Figure 4. A higher concentration of silicon and lower concentration of calcium for the straw mixtures are noticeable, as compared to the pure grot.

dx.doi.org/10.1021/ef200232r |*Energy Fuels* 2011, 25, 2687–2695

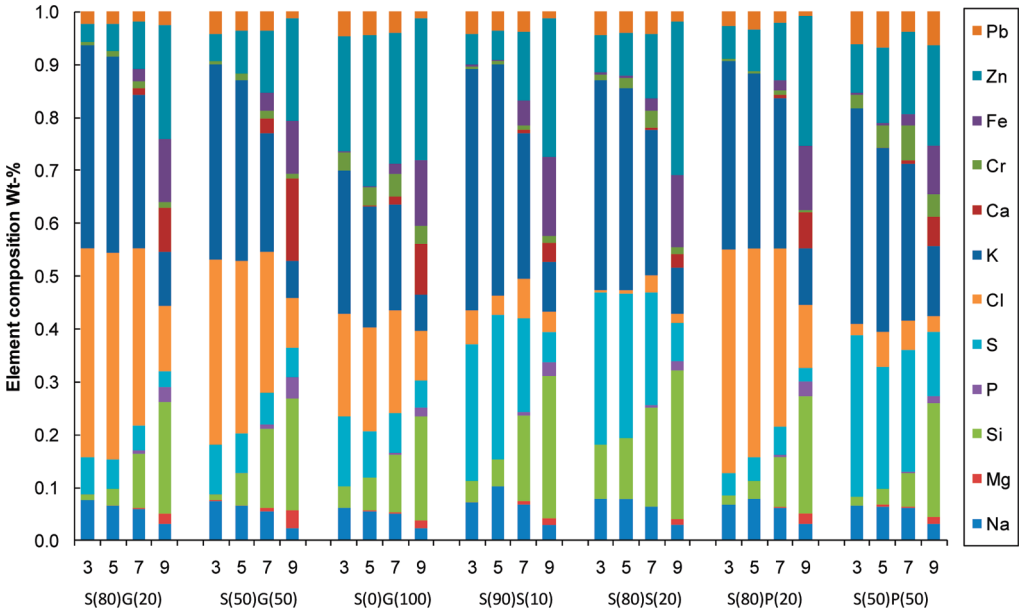

Figure 6. Elemental composition of the aerosols (the impactor stages 3, 5, 7, and 9) corresponding to the sizes 0.093, 0.26, 0.611, and 1.59 μm of the fly ash taken by the ELPI in the exhaust of the reactor, in weight percent for all of the experiments (G, grot; S, sewage sludge; and P, peat).

It is also worth mentioning that the concentration of sulfur and chlorine in the bottom ash is low, which stresses the fact that their volatilities during combustion are high. The bottom ash composition of the straw/sludge mixtures differs from the rest of the mixtures in their higher phosphorus and iron contents. The effect of the fuel interaction is not possible to determine from this figure alone; however, the effect of fuel mixtures of some important elements is discussed later in more detail.

Aerosol Size Distribution and Composition. The experiments with the straw/grot mixtures (top graph of Figure 5) give similar results for the particle concentration, producing a peak at a particle diameter of 0.12 μm. In comparison to experiments with pure grot, the peak concentration for the mixtures is more than doubled and lies close to $4 \times 10^7/\mathrm{cm}^3$. The peak concentration value is shifted toward larger particle diameters with pure grot compared to the straw/grot mixtures (from 0.12 to 0.20 μm). On the basis of the results of the fine particle emissions of the straw/grot mixtures, it can be concluded that grot may not be a proper fuel mixing choice for corrosion reduction in straw combustion for two reasons. First, grot does not appear to have any significant particle load reduction effect with straw. Second, it seems that not even a dilution effect is observed in the mixtures. This nonlinear effect indicates that the aerosol-forming chemistry is actually affected negatively by grot−straw interactions. A broader comparison to the combustion of 100% straw was unfortunately not possible because of severe problems with ash sintering on the grate, which prevented us from collecting reliable experimental results. The graph on the bottom left of Figure 5 represents the results with straw/sludge mixtures. The particle concentration for this series is significantly lower than for the straw/grot mixture and is close to the concentration of the pure grot experiment. Fewer problems related to chlorine corrosion from the sludge mixtures can be expected because sub-micrometer particles have high concentrations of alkali chlorides (in comparison to coarse particles). It is also interesting to point out that the shape of the curves appears to be bimodal, with the first peak at a particle size diameter of 0.04 μm and the second peak at a particle size diameter of 0.2 μm. The bimodal type of particle emission might be caused by different mechanisms of particle formation. The increase of the sewage sludge share from 10 to 20% in the straw substantially decreases the particle load in the flue gas. Most of the reduction occurs in the lower range of the particle size diameter and up to the point where the first peak is almost eliminated. The graph in the bottom right of Figure 5 shows the effect of peat addition on the particle load during straw/peat combustion. For 20% addition with straw, the particle concentration ranking is grot > peat > sewage sludge, and this classification can be said to directly reflect the corrosion reduction efficiency of these additional fuels to straw. For peat, an additional increase to 50% was able to further decrease the particle load. As opposed to the bimodal particle emission of the mixtures with sewage sludge, the emission profile for the peat mixtures is unimodal.

Figure 7 shows the resulting chemical compositions of selected aerosol fractions from the straw/grot experiments. The salt part is very rich in chlorides because over 70% of the salt metals are bound to chlorine for the 20% mixture. Increasing the grot share in the straw is slightly decreasing the chlorides and increasing the sulfates. For the experiment with pure grot, the salt metals are evenly distributed between chlorides and sulfates. It is also worth noticing that zinc chloride or sulfate is largely represented among the salts, and its concentration is increasing with an increasing particle size. The ratio between sodium and potassium is rather constant (1:2−3). However, in all of the mixtures, the portion of potassium decreases with an increasing particle size. For all experiments, lead is only present in marginal quantities. The chemical compositions of selected aerosol fractions for sewage sludge/peat mixtures are shown in Figure 8. For the sewage sludge mixtures, the chlorides are considerably reduced, as compared to grot addition at 10 wt %. Increasing the sludge to 20 wt % is almost completely eliminating chlorides from the aerosols. The results indicate that the smaller particles have fewer chlorides than the larger particles. The salt part

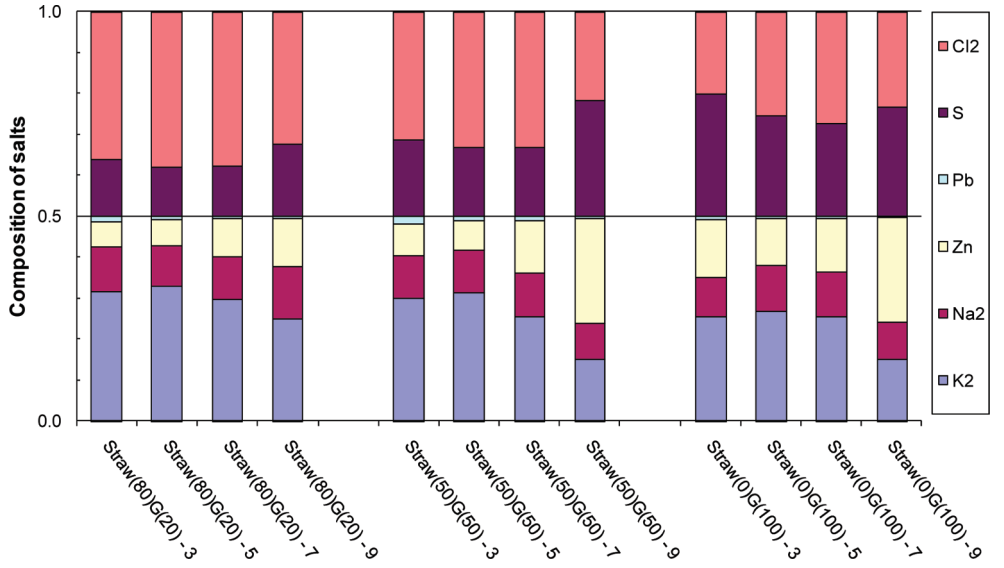

Figure 7. Chemical composition of the aerosols (impactor stages 3, 5, 7, and 9) corresponding to the sizes 0.093, 0.26, 0.611, and 1.59 μm of the fly ash taken by the ELPI in the exhaust of the reactor for the straw/grot (G) fuel mixtures.

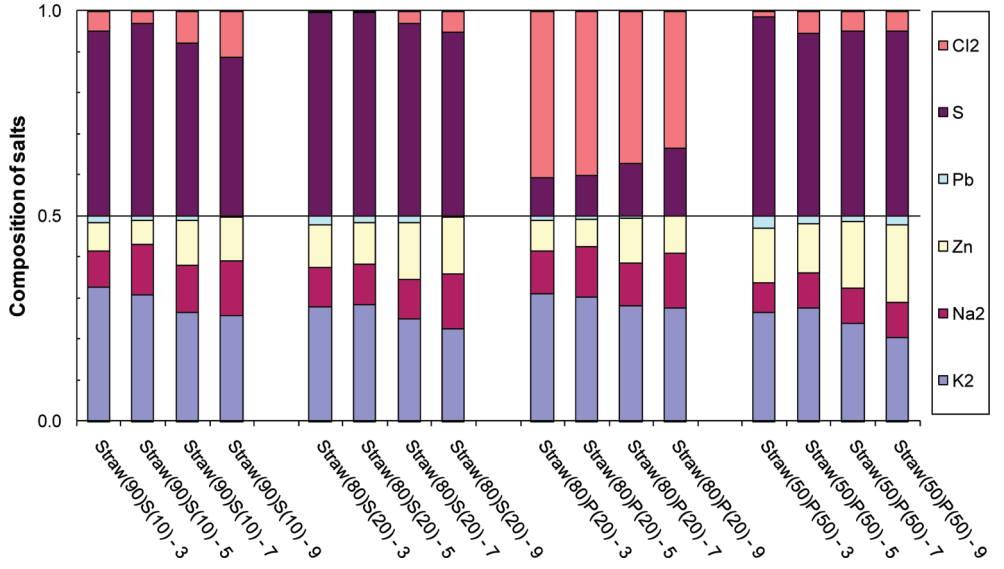

Figure 8. Chemical composition of the aerosols (impactor stages 3, 5, 7, and 9) corresponding to the sizes 0.093, 0.26, 0.611, and 1.59 μm of the fly ash taken by the ELPI in the exhaust of the reactor for the straw/sewage sludge (S) and the straw/peat (P) fuel mixtures.

consists of approximately 60% potassium sulfates, and the rest are equally distributed between zinc and sodium sulfates. With 20 wt % peat addition, the chlorides are dominating, much higher than for the 50% grot addition, but comparable to the 20% addition. For the experiment with 50% peat addition, the chlorides are dramatically reduced. The salt metal composition is more or less comparable to experiments with sludge addition. However, an increase in zinc and lead is noticed for the experiment with 50% peat addition. The greatly reduced chloride amounts at 50% peat addition might reduce the overall corrosion risk in boilers, but the higher Zn and Pb concentrations may lead to higher melt fractions in the aerosols, a factor which could significantly worsen the corrosion risk.

Fate of Chlorine. The chlorine distribution among the solid phase (bottom ash) and the gas phase is shown in Figure 9. This figure does not include the chlorine part found in the fly ash because only some impactor stages were analyzed. However, the amount of chlorine found in the fly ash is most likely very low and thus of little significance to the total Cl mass balance. HCl (gas) accounts for approximately 80% of the chlorine found in the fuel. Chlorine retained in the bottom ash after combustion is quite low for all experiments but increases with increased proportions of secondary fuel. The most noticeable chlorine retention can be seen for 50% peat addition, where 20% of the chlorine found in the mixture is retained in the bottom ash. About 20% of the Cl is unaccounted for because of experimental uncertainties, except for the 50% peat in straw experiment, where the unaccounted Cl value is below 10%.

Fate of Sulfur. A similar mass balance is presented in Figure 10 for sulfur. The results are somehow more scattered than the ones

dx.doi.org/10.1021/ef200232r |*Energy Fuels* 2011, 25, 2687–2695

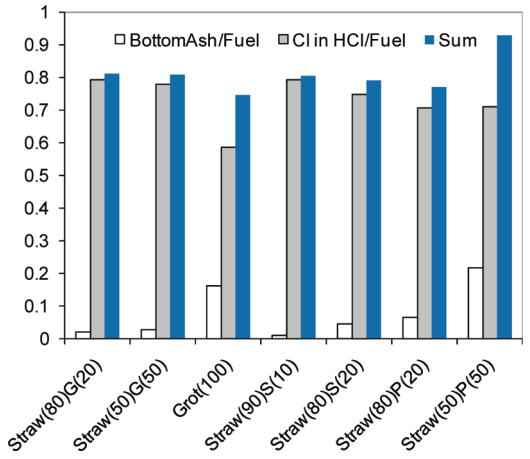

Figure 9. Chlorine distribution in the gas, the bottom ash, and (part of the) fly ash phase for all of the experiments (for the *x* axis, G, grot; S, sewage sludge; and P, peat).

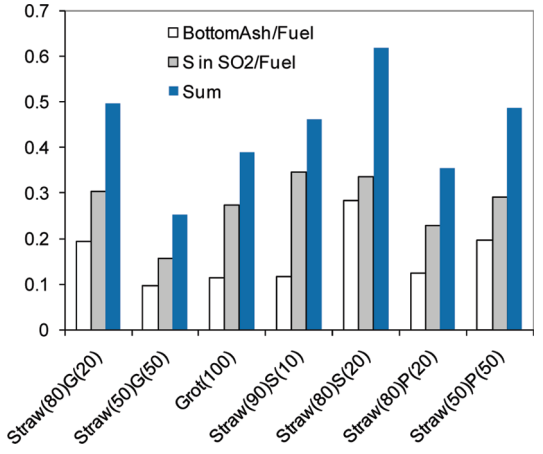

Figure 10. Sulfur distribution in the gas, the bottom ash, and (part of) the fly ash phase (for the *x* axis, G, grot; S, sewage sludge; and P, peat).

from the chlorine balance. The sulfur shares in the gas phase (as SO_2) and in the bottom ash are varying between 25 and 60%, as a function of the fuel mixtures. An increasing retention of sulfur in the bottom ash with increasing sludge and peat addition is clearly observed, while the opposite effect seems to occur with grot addition.

Potassium and Sodium Retention. As already mentioned, the combination of high contents of both alkali metals and chlorine in straw makes the combustion process very challenging. Preventing alkali chlorides from exiting the combustion chamber is regarded as the most effective measure for avoiding corrosion in boilers. Increased alkali capture in the bottom ash should therefore directly translate into a decreased corrosion risk. In Figure 11, the retention of potassium and sodium in the bottom ash relative to quantities in the raw fuel is presented. The results for potassium can be described as such: (1) K retention is about 80% or more for most of the experiments in this study; K can therefore be described as a moderate to nonvolatile compound. (2) Increasing proportions of added fuels improve K retention in the bottom ash to about 100% in two cases: 20% sewage sludge and 50% peat (with straw as the main fuel). Grot only increases K retention to about 90% at a 50% addition level. The trends of

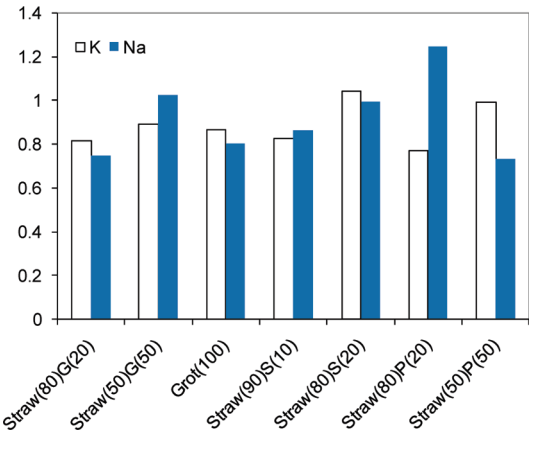

Figure 11. Potassium and sodium retention in the bottom ash for all of the experiments. (for the *x* axis, G, grot; S, sewage sludge; and P, peat).

sodium retention in the bottom ash are very similar to the potassium, except for peat addition, where opposite trends are observed. Sodium is usually omitted from discussions in scientific journals, mainly because it is present in lower quantities (see Table 3) in biomass, which make its effect on corrosion insignificant compared to potassium. The low concentration of sodium in the raw fuel could also explain the higher uncertainty in the mass balance calculation.

CONCLUSION

Several promising secondary fuels to be added to straw have been tested to abate Cl-induced corrosion straw during combustion. The goal was to capture alkali metals in the bottom or fly ash, i.e., preventing the formation of corrosive alkali chlorides and promoting the formation of noncorrosive gaseous hydrogen chloride. Three supplementary fuels were used: grot, sewage sludge, and peat. Binary mixtures with different mixing ratios were combusted in a multi-fuel laboratory reactor under controlled conditions: (1) The concentrations of the most relevant gaseous species were monitored. (2) The aerosol size distribution and the chemical composition of selected sub-micrometer particles in the flue gas were measured. (3) The chemical composition of the bottom ash and in the raw fuel mixtures was analyzed. The relative corrosion risk of the different fuel mixtures was classified on the basis of a careful observation of the measured data. The following conclusions are drawn: (i) The different fuel mixtures had a wide variation in the ash composition, which made the interpretation of the combustion results quite interesting relative to the type and amount of the supplements used. (ii) Although the heterogeneous fuel was fed in a semi-continuous manner to the reactor, the measured combustion parameters showed good control over the process, where results were found to be consistent relative to time variation. (iii) The particle load in the flue gas was strongly influenced by sewage sludge, where a 10% addition resulted in a 65% decrease in the particle concentration in the flue gas compared to the fuel mixture of straw and 20 wt % grot. The reference experiment with pure straw could not be used as a baseline because of sintering problems, which rendered this experiment impossible to run in a reliable way. Grot, on the other hand, was not good as a fuel additive with straw because the aerosol load was influenced negatively at increased addition. Peat had a positive effect on decreasing the particle load, although an addition of 50% was

needed to obtain similar results to the 20% sludge addition. (iv) The potential of chlorine corrosion could be best predicted through the results of the chemical composition of the aerosols. The grot addition was deemed to have an insignificant effect on reducing the alkali chloride concentration in the flue gas. Peat was found to contribute to a reduced corrosion environment only when highly supplemented to straw (50 wt %). The higher zinc concentration at this level of peat addition may reduce the overall effect gained in the reduced content of alkali chlorides. The sewage sludge addition was very effective at reducing the alkali chlorides at 10% addition and almost eliminating them at 20% addition. (v) The chlorine and sulfur distribution were calculated for all of the experiments and showed consistency with the other results concerning the corrosion risk, emphasizing the quality of the experiments.

AUTHOR INFORMATION

Corresponding Author

*E-mail: roger.a.khalil@sintef.no.

ACKNOWLEDGMENT

The work is financed by the Research Council of Norway and a number of industrial partners through the projects KRAV ("Enabling Small Scale Biomass CHP in Norway") and CenBio (Bioenergy Innovation Centre). We also thank BIOENERGY 2020+, Austria, and DTU, Denmark, for providing fuels and related fuel data through the SciToBiCom ERA-net.

REFERENCES

(1) International Energy Agency (IEA). *World Energy Outlook 2009*; IEA: Paris, France, 2009.

(2) Yin, C.; Rosendahl, L. A.; Kaer, S. K. *Prog. Energy Combust. Sci.* **2008**, *34* (6), 725–754.

(3) Coda, B.; Aho, M.; Berger, R.; Hein, K. R. G. *Energy Fuels* **2001**, *15* (3), 680–690.

(4) Nielsen, H. P.; Frandsen, F. J.; Dam-Johansen, K.; Baxter, L. L. *Prog. Energy Combust. Sci.* **2000**, *26* (3), 283–298.

(5) Davidsson, K. O.; Amand, L. E.; Steenari, B. M.; Elled, A. L.; Eskilsson, D.; Leckner, B. *Chem. Eng. Sci.* **2008**, *63* (21), 5314–5329.

(6) Becidan, M.; Sørum, L.; Lindberg, D. *Energy Fuels* **2010**, *24* (6), 3446–3455.

(7) Riedl, R.; Dahl, J.; Obernberger, I.; Narodoslawsky, M. Corrosion in fire tube boilers of biomass combustion plants. *Proceedings of the China International Corrosion Control Conference '99*; China Chemical Anticorrosion Technology Association (CCATA), Beijing, China, 1999; Paper 90129.

(8) Obernberger, I.; Brunner, T.; Bärnthaler, G. *Biomass Bioenergy* **2006**, *30* (11), 973–982.

(9) Dayton, D. C.; Jenkins, B. M.; Turn, S. Q.; Bakker, R. R.; Williams, R. B.; Belle-Oudry, D.; Hill, L. M. *Energy Fuels* **1999**, *13* (4), 860–870.

(10) Salour, D.; Jenkins, B. M.; Vafaei, M.; Kayhanian, M. *Biomass Bioenergy* **1993**, *4* (2), 117–133.

(11) Steenari, B. M.; Lindqvist, O. *Fuel* **1999**, *78* (4), 479–488.

(12) Pettersson, A.; Zevenhoven, M.; Steenari, B. M.; Amand, L. E. *Fuel* **2008**, *87* (15−16), 3183–3193.

(13) Munir, S.; Nimmo, W.; Gibbs, B. M. *Energy Fuels* **2010**, *24*, 2146–2153.

(14) Davidsson, K. O.; Amand, L. E.; Elled, A. L.; Leckner, B. *Energy Fuels* **2007**, *21* (6), 3180–3188.

(15) Aho, M.; Yrjas, P.; Taipale, R.; Hupa, M.; Silvennoinen, J. *Fuel* **2010**, *89* (9), 2376–2386.

(16) Spliethoff, H.; Scheurer, W.; Hein, K. R. G. *Process Saf. Environ. Prot.* **2000**, *78* (B1), 33–39.

(17) Lundholm, K.; Nordin, A.; Ohman, M.; Bostrom, D. *Energy Fuels* **2005**, *19* (6), 2273–2278.

(18) Davidsson, K. O.; Steenari, B. M.; Eskilsson, D. *Energy Fuels* **2007**, *21* (4), 1959–1966.

(19) Vamvuka, D.; Zografos, D.; Alevizos, G. *Bioresour. Technol.* **2008**, *99* (9), 3534–3544.

(20) Boström, D.; Grimm, A.; Boman, C.; Björnbom, E.; Öhman, M. *Energy Fuels* **2009**, *23* (10), 5184–5190.

(21) Bartels, M.; Lin, W. G.; Nijenhuis, J.; Kapteijn, F.; van Ommen, J. R. *Prog. Energy Combust. Sci.* **2008**, *34* (5), 633–666.

(22) Khalil, R.; Todorovic, D.; Skreiberg, Ø.; Becidan, M.; Backman, R.; Goile, F.; Skreiberg, A.; Sørum, L. The effect of kaolin on the combustion of demolition wood under well controlled conditions. *Waste Manage. Res.*, **2011**, manuscript submitted for publication.

(23) Backman, R.; Khalil, R.; Todorovic, D.; Skreiberg, Ø.; Becidan, M.; Goile, F.; Skreiberg, A.; Sørum, L. The effect of peat ash addition to demolition wood on the formation of alkali, lead and zinc compounds at staged combustion conditions. *Fuel Process. Technol.* **2011**10.1016/j.fuproc.2011.04.035.

(24) Kassman, H.; Bafver, L.; Amand, L. E. *Combust. Flame* **2010**, *157* (9), 1649–1657.

(25) Aho, M.; Vainikka, P.; Taipale, R.; Yrjas, P. *Fuel* **2008**, *87* (6), 647–654.

(26) Broström, M.; Kassman, H.; Helgesson, A.; Berg, M.; Andersson, C.; Backman, R.; Nordin, A. *Fuel Process. Technol.* **2007**, *88* (11−12), 1171–1177.

(27) Elled, A. L.; Amand, L. E.; Leckner, B.; Andersson, B. A. *Fuel* **2006**, *85* (12−13), 1671–1678.

(28) Grimm, A.; Skoglund, N.; Boström, D.; Öhman, M. *Energy Fuels* **2011**, *25*, 937–947.

(29) Elled, A.-L.; Davidsson, K. O.; Åmand, L.-E. *Biomass Bioenergy* **2010**, *34* (11), 1546–1554.

(30) Åmand, L. E.; Leckner, B.; Eskilsson, D.; Tullin, C. *Fuel* **2006**, *85* (10−11), 1313–1322.

(31) Aho, M.; Silvennoinen, J. *Fuel* **2004**, *83* (10), 1299–1305.

(32) Becidan, M.; Houshfar, E.; Khalil, R.; Skreiberg, Ø.; Sørum, L. Optimal biomass mixtures to reduce corrosion and deposition: A thermodynamic analysis. *Energy Fuels* **2011**, manuscript submitted for publication.